Continental Shelf Research, Vol. 12, No. 4, pp. 499–515, 1992.
Printed in Great Britain.

0278–4343/92 $5.00 + 0.00

Subtidal currents from a shipboard acoustic Doppler current profiler in tidally dominated waters

ANDREAS MÜNCHOW,* RICHARD W. GARVINE* and TIMOTHY F. PFEIFFER*

(*Received* 30 *January* 1991; *accepted* 18 *March* 1991)

Abstract—As part of a comprehensive study of inner shelf dynamics in the vicinity of a major estuary, we test the performance of a shipboard acoustic Doppler current profiler (ADCP). We compare velocities from the ADCP with those from current meters located 6 and 10 m below the surface in water shallower than 30 m. We find the ADCP suitable to estimate subtidal currents of O(10 cm s^{-1}) embedded in a tidal flow exceeding 100 cm s^{-1}. We obtain the former currents by subtracting predicted tidal currents which we computed from empirical models. Three different models all result in similar subtidal flows; none of them appears superior. However, spatial and temporal averaging of the velocity data are necessary to reduce noise in the ADCP record to acceptable levels. Our subtidal flow estimates are reliable, robust and physically meaningful. We find that bottom friction influences the tidal currents over the entire water column. We also find a narrow, baroclinic, subtidal jet exiting the estuary on the right looking seaward. This jet is the source of the local buoyancy-driven coastal current.

1. INTRODUCTION

THE introduction of a practical acoustic Doppler current profiler (ADCP) has strongly affected research in physical oceanography because of the detailed and extensive data it returns. REGIER (1982) pioneered the use of a shipboard ADCP in studies of open ocean mesoscale variability. Since then, the ADCP has found a wide range of applications, such as Gulf Stream transects (BEREZUTSKII *et al.*, submitted), cold outflows through the Faroe Channel (SAUNDERS, 1990), coastal upwelling systems (BARTH and BRINK, 1987; KOSRO, 1985), and tidal flows around headlands (GEYER and SIGNELL, 1990). A major advantage of coastal ADCP applications is that one generally obtains accurate velocity vectors because the bottom can be tracked at all times. The major disadvantage, though, is that often the desired low-frequency (subtidal) signal is masked by strong tidal motion.

Only recently, researchers began to address this problem and to attempt to remove tidal currents from ADCP records. GEYER and SIGNELL (1990) and SIMPSON *et al.* (1990) analysed repeated transects over one or more tidal cycles. CANDELA *et al.* (1990) proposed a different method that requires no repetition, thus reducing expensive ship time. While the former authors fitted sinusoidal tidal variations to ADCP data at discrete points in a profiling transect, CANDELA *et al.* (1990) prescribe spatial base functions which simulate the horizontal distribution of tidal properties. FOREMAN and FREELAND (1992) used a numerical model to remove undesired tidal velocities from a 3 day ADCP record off

*College of Marine Studies, University of Delaware, Newark, DE 19716, U.S.A.

British Columbia, Canada. Here we will compare the subtidal currents which we obtain from an ADCP record applying the repeated transect and the spatial base function method, and a third one where we interpolate tidal currents from nearby current meters to our measurement locations. Details of these methods we discuss in Section 3.

This study is part of a comprehensive observational study of inner shelf dynamics in the vicinity of a major estuary, Delaware Bay, U.S.A. The water depths are less than 30 m. Tidal currents are of the same order as the subtidal ones (20 cm s^{-1}), except near the mouth of the estuary where they exceed 100 cm s^{-1}. Therefore, we choose the mouth of the estuary to compare the above methods. We will stress the physical soundness and consistency of the obtained tidal and subtidal velocity estimates by explaining observed circulation qualitatively. We defer a detailed, dynamical analysis of the data to a subsequent paper. Instead, our focus here is on the performance and reliability of an ADCP to measure subtidal currents in a tidally dominated environment.

In Section 2 we compare the ADCP with current meter data on the shelf, derive an objective screening criteria, and discuss possible error sources. In Section 3 we will then describe the methodology of detiding the ADCP record and present the tidal flow field at the mouth of Delaware Bay. We find that frictional dynamics dominate. Finally, in Section 4 we compare the subtidal flows resulting from the different detiding methods and stress the consistency of the subtidal flow with the density field. Section 5 concludes the paper.

2. COMPARISON WITH CURRENT METERS

Aboard the R.V. *Cape Henlopen* we used a hull-mounted 307 kHz ADCP of RDI Inc. on transects A, B and C shown in Fig. 1. Pertinent details of the ADCP set-up and its calibration we list in Table 1. We found the ADCP data and the bottom tracking to degrade at ship speeds larger than 2 m s^{-1}. Therefore, we moved at a constant speed of about 1.5 m s^{-1} with no change in direction. We averaged the velocity estimates vertically into 2 m bins, the first one starting 4 m below the surface. The transducer depth was 1 m. Because of acoustic sidelobe interference near the bottom in conjunction with heavy seas, we discarded all data originating from within 0.25 H of the bottom where H is the local water depth. For each discrete station we averaged the ADCP data aquired over 10 min. Each velocity estimate thus corresponds to a spatial average along the ship track of almost 1 km. Transect B near the mouth of the estuary consists of nine such stations, while transects A and C on the inner shelf off New Jersey and Delaware, respectively, consist of eight stations each.

We will compare the ADCP velocity estimates to current estimates from 10 current meters at the six mooring locations shown in Fig. 1. The current meters were the InterOcean S4 type which we set on moorings at 6 and 10 m depth. Every half hour the S4 current meters sampled velocity vectors at 2 Hz for 5 min, vector averaged them over this period, and stored the averaged vector only. Some mismatch of spatial and temporal sampling scales is thus evident. We compare velocity data cautiously from these two different sources and then only when the ship was within 1 km of a mooring location.

Next we establish a screening criterion in order to remove spurious data objectively. The ADCP consists of four downward-looking transducers from which it computes three velocity components. One obtains two independent estimates of the vertical velocity component whose difference has been interpreted as an error velocity V_e (DIDDEN, 1987). Another variable related to ADCP data quality control is the fraction of the received

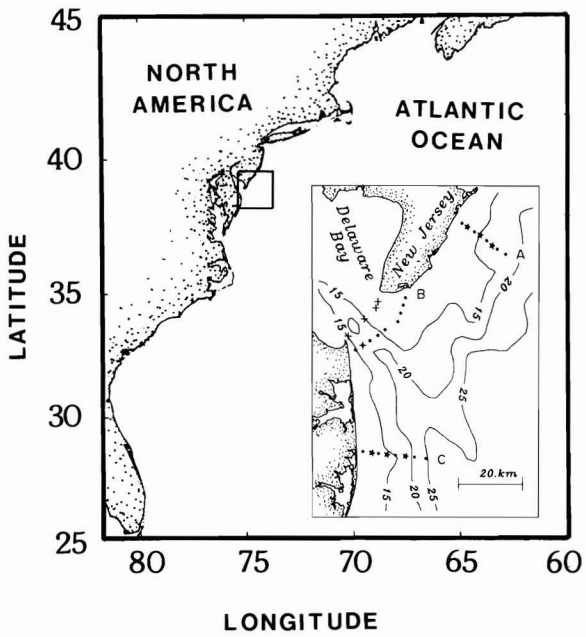

Fig. 1. Map of the study area. The insert is an enlargement of the rectangle at 39°N latitude and 75°W longitude. The insert shows the bathymetry in meters and the ADCP stations on transects A (off New Jersey), B (mouth of Delaware Bay), and C. The star symbols represent S4 current meter mooring locations which we maintained while profiling with the ADCP. Dots indicate ADCP profiling stations and crosses mark the location of historical current meter moorings.

acoustic pings that exceed a signal to noise ratio of 6 dB. This variable we abbreviate as P_g (for "per cent good pings"). We decompose the S4 and ADCP estimates of the velocity vector into speed and direction and show the speed difference of the two in Fig. 2a and b as a function of V_e and P_g, respectively. The speed difference scatters almost uniformly as a function of V_e (Fig. 2a) while it is highly concentrated as a function of P_g (Fig. 2b). The

Table 1. *ADCP properties*

Acoustic frequency	307 kHz
Ping rate	1 Hz
Vertical bin size	2 m
Pulse length	2 m
Transducer depth	1 m
Blanking below transducer	3 m
Time average	10 min
Ship speed	1.5 m s^{-1}
Horizontal sampling	1 km
Firmware version	15.88
DAS software version	2.28
Transducer misalignment α*	1.7°
Sensitivity constant β*	0.9947

*Calibration coefficients (Joyce, 1989).

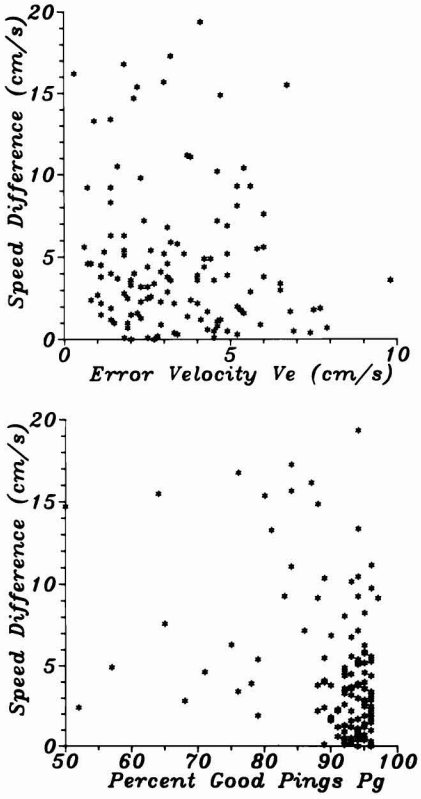

Fig. 2. Speed difference between S4 current meter and ADCP data (see Fig. 1 for locations) as a function of (a) V_e, an error velocity; (b) P_g, the "per cent good pings". Note the almost uniform scatter of data in (a) but the concentrated distribution in (b).

directional difference as a function of P_g and V_e resembles Fig. 2 but is not shown. Hence, we discard V_e but retain P_g for further use as a screening variable.

We now decompose the velocity difference vector into along- and across-ship components. We then plot P_g as a function of these components in Fig. 3. The symbols indicate the data points from which the contours have been computed. Most of the data are near zero velocity differences and where $P_g > 90$. Figure 4 compares directly the S4 against ADCP velocity data. Notice that most of the differing velocities occur in the along-ship, not the across-ship component. Next we will discuss the bias and scatter of these distributions in detail.

JOYCE (1989) outlined an ADCP calibration routine which we followed closely. He introduced two parameters, each of which describes approximately the error of one horizontal velocity component. A transducer misalignment causes errors dominantly in the across-ship velocity component, while a scaling or sensitivity error causes errors dominantly in the along-ship component. In Table 2 we present the velocity bias and scatter of the ADCP data relative to the S4 data along with the dominant wind and wave conditions for two field experiments. We define the bias and scatter as the mean and standard deviation, respectively, of the difference between the S4 and ADCP velocity

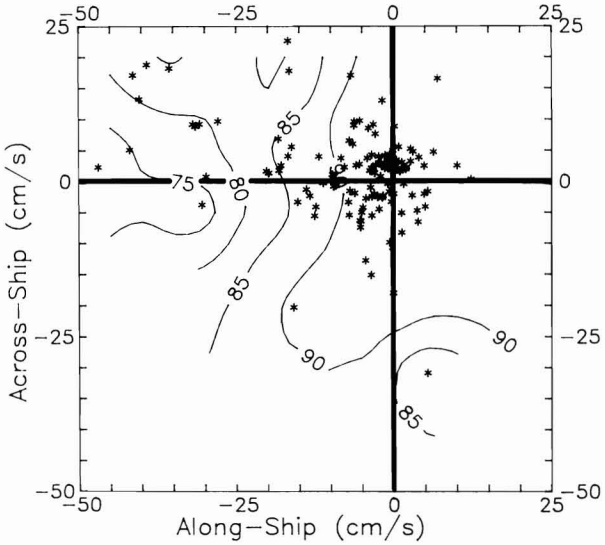

Fig. 3. The "per cent good pings" P_g as a function of along- and across-ship velocity difference between S4 current meter and ADCP velocity data. The symbols indicate data points. Note that large velocity differences occur dominantly at lower P_g and in the along-ship velocity component.

estimates. Notice that the along-ship bias is several times that of the across-ship bias. Why? The ADCP measures the bottom and the water velocity relative to the moving transducers. Neglecting the sensitivity error for the moment, we reason that a transducer misalignment will cause a constant directional off-set for each measured velocity vector. The absolute velocity vector is the difference between the water and the bottom velocity relative to the transducer. This difference vector thus does not contain any misalignment error, since it is invariant under coordinate rotation. Therefore, the across-ship velocity bias is much smaller than the along-ship bias of -3.6 cm s^{-1}, i.e. the S4 estimates are consistently smaller than the ADCP estimates. Calibrating the ADCP according to JOYCE (1989) gives a 1.7° clockwise misalignment and a scaling constant $\beta = 0.9947$. Hence the ADCP overestimates velocity by 0.5% of the ship speed resulting in a bias of 1.5 cm s^{-1}. We computed filter skew bias (CHERESKIN *et al.*, 1989) and found it always less than 1 cm s^{-1}. We are still left with about 1 cm s^{-1} of unexplained bias. In Table 2 we also compare bias and scatter from the two experiments separately and find that the bias is independent of the sea state while the scatter is not. The velocity scatter increases from 5 cm s^{-1} to 9 cm s^{-1} for a doubling of the mean wave height. We thus find about 7 cm s^{-1} of velocity scatter which includes instrument noise ($\approx$1 cm s^{-1} for ADCP and S4 each), physical noise (small scale motion), and undetected errors due to the ship's gyro, ship's pitch and roll, ship's engine vibrations, and errors due to air bubbles near the ship's hull. Note that the scatter is about the same for the along- and across-ship velocity component, unlike the bias.

A 3.6 cm s^{-1} velocity bias may render some of our results ambiguous. We note, however, that we did not perform any subjective data editing. If we do discard about 5% of the data subjectively, the bias and scatter drop by a factor of three and two, respectively. Nevertheless, in all the following we retained all data which passed our screening criteria $P_g > 85$.

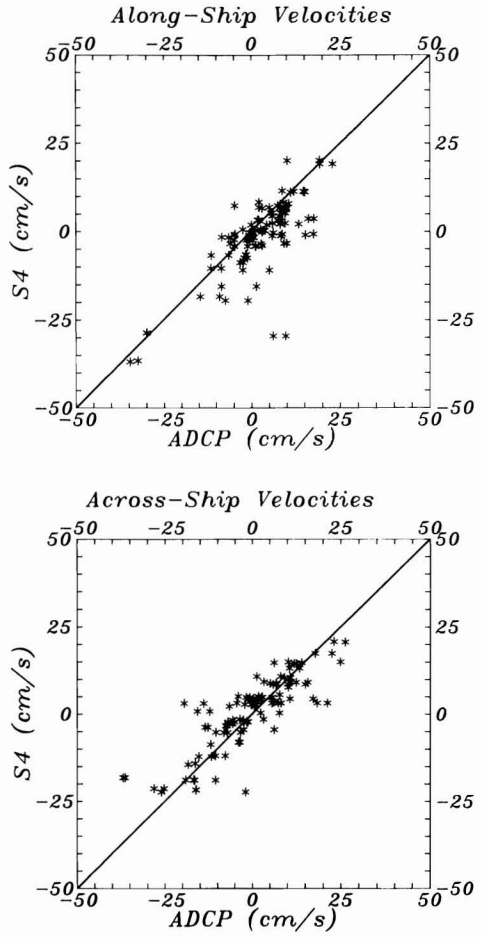

Fig. 4. Direct comparison of S4 current meter and ADCP data for which P_g exceeds 85. The straight line indicates perfect agreement.

Our hull-mounted ADCP overestimates currents in waters less than 30 m deep with an unexplained bias of about 1 cm s^{-1}. We found a useful objective screening criterion to be the fraction of pings P_g exceeding a signal to noise ratio of 6 dB and thus rejected data with $P_g < 85$. As KOSRO (1985), BARTH and BRINK (1987), and GEYER and SIGNELL (1990) we

Table 2. Velocity bias and scatter for* $P_g > 85$

Experiment	Along-ship (cm s^{-1})	Across-ship (cm s^{-1})	N	Wave height (m)	Wind (m s^{-1})
April	-3.3 ± 5.3	1.2 ± 4.1	58	0.7	2
June	-3.9 ± 9.5	1.2 ± 9.4	37	1.5	5
Mean	-3.6 ± 7.4	1.2 ± 6.9	95	—	—

*Standard deviation.

find rather large velocity scatter, thus some spatial or temporal averaging is necessary to reduce the errors associated with it.

3. TIDAL CURRENTS

Our goal is to extract a subtidal velocity signal from ADCP records which are heavily contaminated by tidal currents. The semi-diurnal frequency band contains about 50% of the total current variance on the inner shelf of the Mid-Atlantic Bight and about 90% near the mouth of Delaware Bay. We choose to study transect B across the mouth of the Delaware Bay (see Fig. 1 for location) because of its strong, spatially variable tidal signals (MÜNCHOW *et al.*, 1992). We first review three different methods, all of which attempt to remove the deterministic tidal signal from the ADCP velocity record. Thereafter, we discuss and explain tidal current ellipses which we obtain from one of the methods. The subtidal velocity field we compute by subtracting the tidal velocity estimates from the raw ADCP data.

Methods to remove tidal currents

The ADCP measures velocity at discrete locations (x_i, z_j) where x_i and z_j represent the horizontal and vertical coordinate, respectively. SIMPSON *et al.* (1990) proposed the first model we tested

$$\psi(x_i,z_j,t) = A_{ij} \cos(\omega t) + B_{ij} \sin(\omega t) \tag{1}$$

where ψ is a velocity component, ω a tidal frequency, and t time, while A_{ij} *and* B_{ij} denote constant coefficients to be determined by least squares fitting. In principle, one can compute A_{ij} and B_{ij} from just two realizations of $\psi(x_i,z_j,t)$, but in practice one needs many more. We required at least five measurements over two semi-diurnal tidal cycles in order to reliably estimate tidal ellipse parameters whose statistical significance we will discuss in the next section.

CANDELA *et al.* (1990) relaxed the requirement of exact repetition of measurements at a location. We followed their work for our second model with

$$\psi(x,z,t) = A(x,z) \cos(\omega t) + B(x,y) \sin(\omega t) \tag{2}$$

where now the coefficients A and B are no longer constants but are linear combinations of arbitrarily prescribed functions $f_i(x,z)$, namely

$$A(x,z) = \Sigma_i \alpha_i f_i(x,z)$$
$$B(x,z) = \Sigma_i \beta_i f_i(x,z).$$

Now the α_i and β_i are constants to which the ADCP data are fitted by least squares. CANDELA *et al.* (1990) successfully applied polynomials and biharmonic splines (SANDWELL, 1987) to a 5-day long ADCP record from the Yellow Sea, China. We choose our base functions to reflect frictional dynamics in the vertical and we modeled horizontal variations as a first order polynomial. Our tidal model thus subjects the ADCP data to equation (2) with

$$A(x,z) = (\alpha_1 + \alpha_2 x)\cos(\zeta)\cosh(\zeta) + (\alpha_3 + \alpha_4 x)\sin(\zeta)\sinh(\zeta)$$

$$B(x,z) = (\beta_1 + \beta_2 x)\cos(\zeta)\cosh(\zeta) + (\beta_3 + \beta_4 x)\sin(\zeta)\sinh(\zeta)$$

where $\zeta \equiv z/\delta_E$ and δ_E is an Ekman layer depth modified by an oscillatory current (PRANDLE, 1982) which depends upon a vertical eddy viscosity (MAAS and VAN HAREN, 1987; EKMAN, 1905). Thus, strictly speaking, δ_E should be another free model parameter, but its inclusion would render the model nonlinear in the parameters, so instead we performed a sensitivity analysis. We varied δ_E from 4 to 400 m and found that the resulting subtidal velocity estimates vary by less than 0.2 cm s^{-1} at any location. Therefore, we conclude that the model is not sensitive to δ_E.

Finally, the third method we used to remove tidal currents utilizes current meter data which the National Ocean Service collected in 1984 for several months at mooring sites near our transect B (crosses in Fig. 1). MÜNCHOW *et al.* (1992) describe the tidal analysis of these data. In Fig. 5 we reproduce the vertical distribution of tidal amplitude and phase along a transect landward about 5 km into the estuary from our ADCP transect B (see Fig. 1 for location): from only seven data points we generated tidal information at more than 150 grid points in the transect which, if contoured, give Fig. 5. Our interpolation scheme utilizes the Golden Software Inc. SURFER program. In essence, at least three data points are required in each of eight angular sectors in an ellipse surrounding a grid point. The data

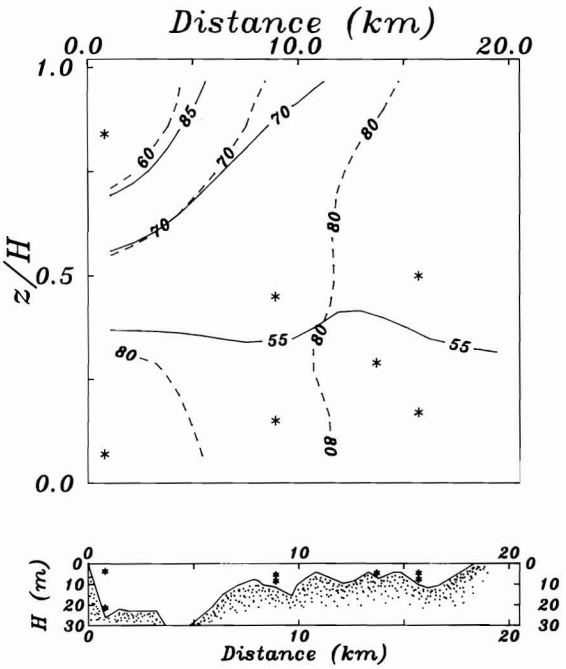

Fig. 5. Values of interpolated M_2 current amplitude on the major axis in cm s^{-1} (solid line) and phase (broken line) on transect B (crosses in Fig. 1) across the mouth of Delaware Bay. Phase angles indicate current lead relative to local coastal sea level. The view is into the estuary with Cape May, New Jersey to the right. The stars mark the location of current meters. The ordinate is z/H where z is measured upward from the bottom and H is the local water depth. In the lower panel we show the distribution of H with distance (from MÜNCHOW *et al.*, 1992).

Table 3. Comparison between ADCP and current meter derived M_2 tidal ellipse parameters

	RMAJ (cm s^{-1})	RMIN	PHASE (°)	ORIE (°)	T (days)	SNR (−)
Current meter	86 ± 0.2	−8	39 ± 4	123	153	1000
ADCP*	98 ± 0.5	−8	63 ± 6	130	2	400
ADCP April:						
Uncorrected	94 ± 4.0	−7	67 ± 16	134	1	50
Corrected	97 ± 4.0	−7	52 ± 16	134	1	50
ADCP June:						
Uncorrected	68 ± 5.0	14	8 ± 21	127	1	30
Corrected	90 ± 5.0	18	4 ± 21	127	1	30

*Harmonic analysis of combined April and June data.

within each ellipse are weighted as the inverse of their distance from the grid point. Finally, we smoothed the entire grid with a horizontal "box car" filter with half-window width $(\Delta x, \Delta z) = (1\text{ km}, 0.05\,H)$ where H is the local water depth. We gridded tidal information for five tidal constituents representing M_2, N_2, S_2, K_1 and O_1 tidal currents.

While the first method is probably the most appealing method from a physical point of view since it is free of subjective choices and interpolation techniques, it is more expensive in ship time, since it takes at least a tidal cycle to resolve tides. We feel that the second method is more restrictive, since spatial base functions have to be prescribed subjectively (CANDELA *et al.*, 1990; FOREMAN and FREELAND, 1992). Finally, the third method requires current meter installation and retrieval, unless historical data are available. Still, some repetition is necessary in order to average over small inaccuracies of the tidal prediction which cause large errors in subtidal velocity estimation. In Section 4 we will find that a single subtidal ADCP speed estimate is accurate only within 10 cm s^{-1} while the average of four estimates is accurate to within 4 cm s^{-1}.

Results

During April and June 1989 the ship moved for about 24 h back and forth on transect B (Fig. 1). On each of the two experiments we obtained up to eight velocity measurements at each of the nine stations on the transect. These 16 or less velocity estimates at each pont (x_i, z_j) within the transect we subjected to least squares harmonic analysis [equation (1)], thus estimating M_2 tidal ellipse parameters. These are the current amplitudes on the major (RMAJ) and minor axes (RMIN), the orientation (ORIE) of the major axis from true east, and the current phase angle (PHASE) at a prescribed time which is the same as used in Fig. 5. The sign of the minor axis indicates the sense of rotation on the ellipse, being positive for cyclonic rotation. By design one of our ADCP stations coincided with the location of a current meter maintained in 1984. If the tidal currents are stationary at this location we can thus directly compare ADCP tidal predictions with those from the current meter moored 4 m below the surface in water 21 m deep. In Table 3 we give the ellipse parameters for the M_2 tidal constituent from the ADCP bin centered 5 m below the surface along with those from the 1984 current meter. Also, we estimate uncertainties in our predictions which are

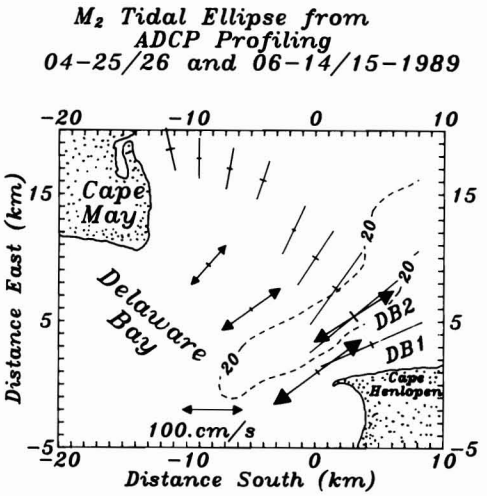

Fig. 6. Near surface M_2 tidal ellipse axes. We show results from both current meter (closed arrow heads) and ADCP data (no arrow heads). The 20 m isobath (dashed line) indicates the position of the deep channel near Cape Henlopen, Delaware (see also Fig. 1 for location).

based on a signal to noise ratio (SNR) criterion given in MÜNCHOW *et al.* (1992). The large SNR of tidal currents at the mouth of the estuary assures statistical significance of ellipse parameters estimated from the short ADCP record. Nevertheless, the ADCP overestimates the M_2 current amplitude on the semi-major axis by about 15%. This is not surprising because the analysis of the 153 days' long current meter record resolves the N_2, S_2 and M_2 tide, while the 2 days' long ADCP record yields only the M_2 for semi-diurnal tides. The phase of the current meter and ADCP data agree to within 24° or about 50 min. Also in Table 3 we give the ellipse parameters for each of the two experiments separately. The differences with current meter data are greater, presumably because of modulations by N_2 and S_2 constituents. SIMPSON *et al.* (1990) following KING *et al.* (1983) proposed an algorithm to correct for a second, unresolved tidal constituent. We applied the algorithm to our data twice in order to correct for N_2 and S_2 tidal currents and show the results labeled "corrected" in Table 3. We find that the amplitude estimation improves while the phase estimation does not.

In Fig. 6 we present the axes of the M_2 tidal ellipses at 5 m below the surface for each station along the transect. Current amplitudes increase almost uniformly from 35 cm s^{-1} near Cape May, New Jersey to 90 cm s^{-1} near Cape Henlopen, Delaware. Here the tidal currents are intensified in the deep channel which acts as the main conveyor of tidal volume entering and leaving the estuary (MÜNCHOW *et al.*, 1992). The axes with closed arrow heads in Fig. 6 are derived from moored current meters near the surface; these compare well with those derived from the ADCP data. The vertical distribution of current amplitudes (RMAJ) and phases in Fig. 7 reveals that currents near Cape May lead those in the deep channel by almost 50° or about 1.5 h. In the deep channel vertical phase differences indicate that bottom currents lead surface currents, but these differences are smaller than the phase uncertainty given for one station in Table 3 and are thus not shown in Fig. 7. We find maximum current amplitudes near the surface over the deep channel. However, comparing the results of Fig. 7 (ADCP data) with those in Fig. 5 (current meter data) the

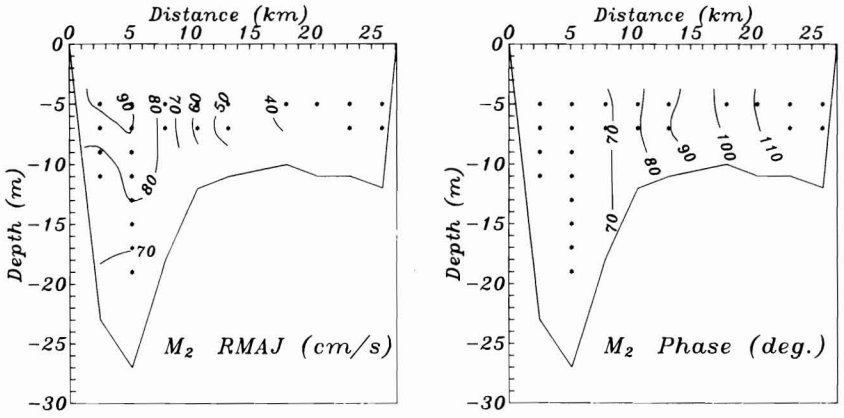

Fig. 7. M_2 current amplitude (RMAJ) and phase on transect B from ADCP data [equation (1)]. Phase angles indicate current lead relative to local coastal sea level (as in Fig. 5). The view is into the estuary with Cape Henlopen on the left and Cape May on the right (see Fig. 1 or Fig. 6 for the locations of ADCP stations). Bottom is shown.

agreement, especially of current phases, is rather poor. We believe that while the ADCP emphasizes the spatial character of tidal currents very well, it fails to resolve other semi-diurnal or diurnal tidal currents. On the other hand, the current meter data resolves the temporal character of tidal currents, but fails to describe tidal currents correct spatially. Thus, Figs 5 and 7 should be compared only with caution. Also, the current meter locations are about 10 km into the estuary from the ADCP station (see Fig. 1) resulting in further phase discrepancy, since the gradients of current phases are large in the study area (MÜNCHOW *et al.*, 1992).

We show the ellipticity of the tidal currents for the two deep channel stations in Fig. 8 as a function of z/H where z is the vertical coordinate and H the water depth. At DB2 tidal currents near the surface rotate anti-cyclonically as indicated by negative ellipticities.

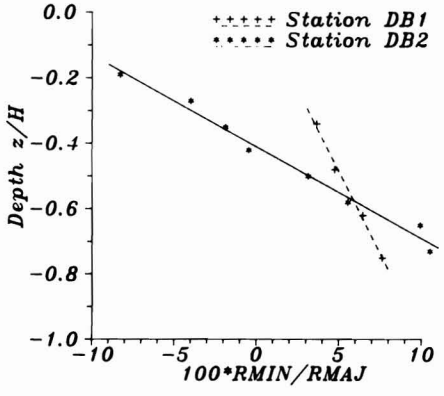

Fig. 8. M_2 ellipticities as a function of depth (scaled by the water depth) for two deep channel stations (see Fig. 6 for locations). Negative ellipticities correspond to anti-cyclonic rotation of the current vector. The lines are linear best fits to the data for each station.

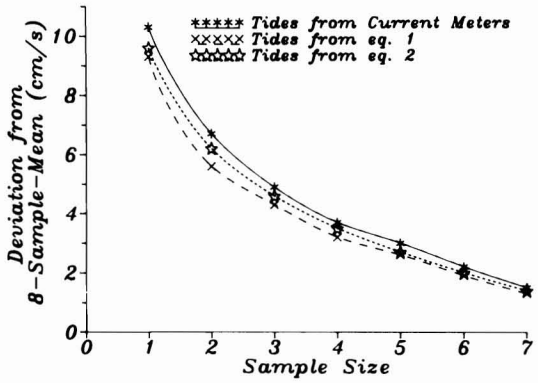

Fig. 9. Subtidal speed deviations from an eight-sample-mean of a randomly sub-sampled and averaged ensemble as a function of sample size. The sample size represents the number of transect repetitions while the deviation from the eight-sample-mean is the speed difference of the sub-sample mean and the mean from eight samples.

Ellipticities increase toward the bottom almost linearly and for station DB2 the sense of rotation changes from anti-cyclonic to cyclonic at $z/H = -0.4$. The maximum ellipticity is always near the bottom. This variation is consistent with the dynamics of a bottom Ekman layer that occupies the entire water column. MAAS and VAN HAREN (1987) report similar results from current meter data in the central North Sea.

We find that the ADCP provides smooth and detailed structure of tides across the channel connecting Delaware Bay with the inner continental shelf. The results agree well with those from current meter data, even though an accurate description of a single tidal constituent phase is not possible in the presence of other tidal constituents of similar frequencies. The vertical current structure is dominated by bottom friction which induces cyclonic motion.

4. SUBTIDAL CURRENTS

At the mouth of Delaware Bay the subtidal circulation is driven by wind and buoyancy forces (GARVINE, 1991) as well as by tidal rectification (MÜNCHOW *et al.*, 1992). Here we show that the ADCP, when operated in shallow (<30 m) water, can reveal such subtidal currents which are embedded in a dominant tidal flow field. Above we introduced three methods of removing tidal currents from the ADCP record. Here, we apply all three methods to our ADCP data and compare the resulting subtidal flows.

In April 1989 we profiled transect B eight times within two tidal cycles. At most points in the transect we thus have eight independent subtidal current estimates after subtracting the tidal current from the raw ADCP data. The average over these eight samples at each point in the transect is equivalent to a least-squares fitted mean current. This eight-sample-mean we now interpret as the "true" current. In order to estimate how the number of transect repetitions affects the subtidal current estimation, we randomly select sub-samples from the eight subtidal current estimates, subtract the mean of the sub-sample from the eight-sample-mean, and plot the results of 1000 different permutations (boot-strapping) in Fig. 9. Because of the boot-strapping each deviation estimate from the eight-

sample-mean in Fig. 9 represents a stable estimate of speed error associated with a finite sample size or transect repetition relative to the eight-sample-mean. We show the results for each of our three detiding methods which all agree to within 1 cm s^{-1} for a given sample size. The results are similar for all sample sizes, i.e. the current meter interpolation method is consistently worse than the spatial base function method, while the harmonic analysis at discrete points performs consistently best. This is not surprising since the current meter moorings were 10 km into the estuary from the ADCP stations, the spatial base functions interpolate tidal currents across the transect, while the last method [equation (1)] fits a tidal model at each point in the transect. Finally, we repeat our earlier statement that while a single subtidal ADCP speed estimate is accurate only within 10 cm s^{-1}, the average of four such estimates is accurate to within 4 cm s^{-1}.

Next, we test the performance of different detiding methods further, each of which should remove about 95% of the current variance at each point (x_i, z_j). However, in order to judge the performance of a detiding method in a bulk sense we interpret every ADCP measurement from transect B as an independent realization of the same point. Thus, we first compute the total bulk variance of the raw data collected in the transect during an experiment. For each of the ADCP data a detiding method predicts a tidal velocity. These tidal velocities we then use to compute the bulk tidal variance. In Table 4 we summarize the ratio of the bulk tidal and the bulk total variance for different detiding methods. There, we also show this ratio for a fourth detiding method, namely removing tidal currents by simply block averaging all available data at a discrete point (x_i, z_j) within the transect. The methods based on equations (1) and (2) can predict the M_2 constituent only, while the third method, which utilizes interpolated current meter data, removes the M_2, S_2, N_2, K_1 and O_1 tidal currents, and the fourth method (averaging) does not discriminate between any tidal constituents. Block averaging currents over a tidal cycle at each point does not remove enough variance (only 33% for the June experiment). Tides predicted from the first three methods all account for roughly 80% of the total variance. We thus still fail to remove all the known tidal variance which at this location is about 95% of the total (MÜNCHOW *et al.*, 1992). However, we still can block average the subtidal velocity estimates from the same observation at each discrete point in the transect. This is equivalent to least squares fitting a mean flow to equations (1) and (2) and removes to some extent diurnal tidal currents as well as inaccuracies in the tidal removal algorithm (Fig. 9). From Table 4 we see (numbers in brackets) that we then remove about 95% of the total variance.

Table 4. *Tidal variance removed (per cent of total) by different detiding methods*

Method applied	April		June	
	(a)	(b)	(a)	(b)
Tides from ADCP data [equation (1)]	79	(93)	86	(97)
Tides from ADCP data [equation (2)]	72	(93)	72	(96)
Tides from current meters data	78	(85)	68	(98)
Block averaging alone	70		33	
Sample size	164	(22)	158	(25)

(a) No averaging.
(b) After averaging subtidal estimates.

Table 5. Subtidal volume transport (10^3 m s^{-1}) across the mouth of Delaware Bay

Method applied	April	June
Tides from ADCP data [equation (1)]	5 ± 3	-2 ± 2
Tides from ADCP data [equation (2)]	3 ± 3	-9 ± 3
Tides from current meter data	2 ± 2	-6 ± 3
Freshwater discharge	0.6	0.8

In Table 5 we give the bulk subtidal volume transport estimates across the transect for the two experiments along with an error estimate due to a 1 cm s^{-1} across-ship velocity error. All values are of the correct order of magnitude. In April we estimate a net outflow of about 2000 m^3 s^{-1} while in June we estimate a net inflow of about 4000 m^3 s^{-1}. All three methods for detiding tidal currents estimate similar subtidal net volume transports whose order of magnitude agree well with flux estimates from much longer current meter time series which we obtained at other times. These fluxes vary on time scales ranging from several days to several weeks, because of time variable buoyancy, wind, and nonlinear tidal forcing (GARVINE, 1991; MÜNCHOW *et al.*, 1992).

A closer look at the spatial distribution of this subtidal outflow reveals intriguing features of a buoyant outflow. Figure 10 depicts the depth averaged subtidal velocity vectors at each station of transect B for April 1989 (tides from current meter data). The outflow concentrates over the deep channel close to the Delaware coast. Over the remainder of the transect the subtidal flow is dominantly across-channel but has a weak component directed into the estuary. The corresponding tidally averaged density section

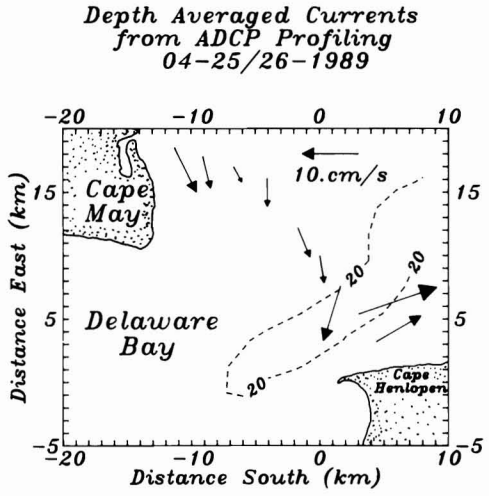

Fig. 10. Depth averaged subtidal velocity vectors across the mouth of Delaware Bay 25/26 April 1989. The tides were removed with data from historical current meter moorings.

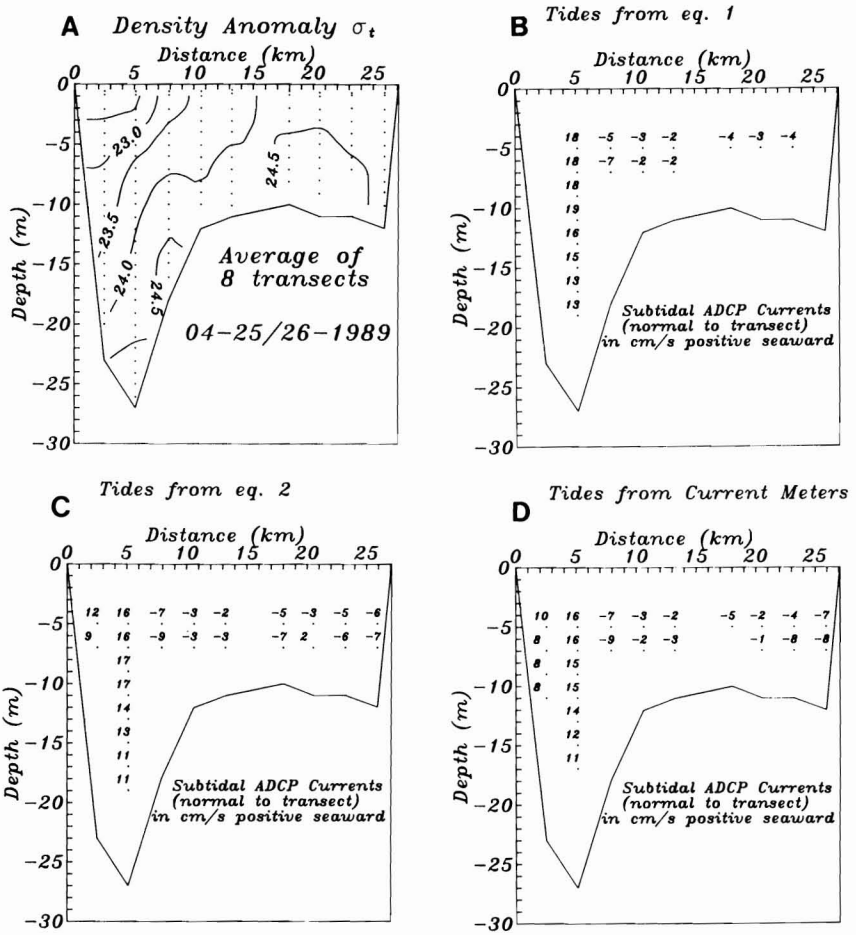

Fig. 11. Vertical distribution of subtidal density anomaly σ_t (kg m^{-3}) and velocity (cm s^{-1}) normal to the transect for 25/26 April 1989: (a) density anomaly σ_t, block average of eight transects; (b) subtidal current speed, tides from ADCP data [equation (1)]; (c) as (b), but tides from ADCP data [equation (2)]; (d) as (b), but tides from current meter data.

(Fig. 11a) confirms this interpretation of a buoyant jet exiting the estuary on the right side looking seaward. The remainder of Fig. 11 shows the vertical distribution of the velocity component perpendicular to the transect, as estimated from each of the three detiding methods. The differences between Fig. 11b [tides from ADCP data subjected to equation (1)], Fig. 11c [tides from ADCP data subjected to equation (2)], and Fig. 11d (tides from current meter data) are minor, thus strengthening confidence in the ADCP estimates. Figure 11 shows that the classical two-layer estuarine gravitational circulation (PRITCHARD, 1956) is absent here. Instead, the buoyant outflow is arranged besides, not above, the heavier inflow. This flow geometry we expect since the width of the estuary exceeds the internal Rossby radius of deformation $\sqrt{g'H}/f$, where g' is the reduced gravity ($g\Delta\rho/\rho$), H and f are the depth and the Coriolis parameter, respectively, and $\Delta\rho$ is a typical vertical

density difference. In this example the internal Rossby radius is about 8 km, while the estuarine width at the mouth is about 25 km.

5. CONCLUSIONS

By comparing our 307 kHz ADCP data against S4 current meter data we found the ADCP to measure currents reliably in shallow waters on the inner continental shelf. The mean along-ship velocity bias of 3.6 cm s^{-1}, however, is too large to be explained by calibration or filter skew error. We probably overestimated velocity bias and scatter, since we applied only one objective data screening criterion. More than half of the bias and scatter originates from only 5% of the record. We were unable to correlate these spurious velocity recordings to any parameter recorded by the ADCP. We used spatial and temporal averaging in order to suppress the random velocity scatter of about 7 cm s^{-1}. This scatter, though, did correlate well with the sea state and was uniform in direction, unlike the bias, which was larger in the along-ship direction.

We compared three methods of detiding current records from ADCP data and found close agreement of subtidal velocity structure. While tidal currents reached 100 cm s^{-1}, subtidal currents did not exceed 20 cm s^{-1}. The observed subtidal flow is consistent with the subtidal density field and subtidal volume transports are of the correct order of magnitude.

We conclude that the shipboard ADCP is an excellent tool to measure spatial variability of both the tidal and the subtidal flow field in the coastal ocean. We demonstrated that one can obtain physically meaningful subtidal current estimates even in the presence of strong tidal currents. The removal of the latter signal was the major objective in the data analysis. Repetitive ship tracks are necessary to reduce some of the tidal noise which remains even after careful detiding. Hence, a carefully chosen ship track and a reliable detiding method are both essential for measuring subtidal currents with an ADCP. We discovered a narrow baroclinic jet which exits the estuary on its right side looking seaward. This jet is the source of the local buoyancy-driven coastal current which transports estuarine material along the coast in the direction of Kelvin wave phase propagation. Future studies will concentrate on these features.

Acknowledgements—We express our gratitude to the crew of the R.V. *Cape Henlopen* under Captain Donald McCann. We also thank members of the scientific party: Leslie Bender III, Claudia and Timothy Ferdelman, Douglas Gaffney, Robert McCarthy, Joy Moses-Hall, and Jürgen Otter. Two anonymous reviewers helped to improve the manuscript with their prompt, pointed, and sympathetic comments. Thomas C. Royer of the University of Alaska, John H. Simpson of the University College of North Wales, U.K. and RDI Inc. all provided initial guidance on the use of the ADCP. This study has been funded by the U.S. National Science Foundation through grant OCE-8816009.

REFERENCES

BARTH J. A. and K. H. BRINK (1987) Shipboard acoustic Doppler profiler velocity observations near Point Conception: spring 1983. *Journal of Geophysical Research*, **92**, 3925–3943.

CANDELA J., R. C. BEARDSLEY and R. LIMEBURNER (1990) *Removing tides from ship-mounted ADCP data, with application to the Yellow Sea*. IEEE Fourth Conference on Current Measurements, pp. 258–266.

CHERESKIN T. K., E. FIRING and J. A. GAST (1989) Identifying and screening filter skew and noise bias in acoustic Doppler current profiler measurements. *Journal of Atmospheric and Oceanic Technology*, **6**, 1040–1054.

DIDDEN N. (1987) Performance evaluation of a ship-board 115 kHz acoustic Doppler current profiler. *Continental Shelf Research*, **7**, 1232–1243.

EKMAN V. W. (1905) On the influence of the earth's rotation on ocean currents. *Arkiv för Matematik, Astronomi och fysik*, **2**, 55–108.

FOREMAN M. G. G. and H. J. FREELAND (1992) A comparison of techniques for tide removal from ship-mounted acoustic Doppler measurements along the south-west coast of Vancouver Island. *Journal of Geophysical Research*, in press.

GARVINE R. W. (1991) Subtidal frequency estuary–shelf interaction: observations near Delaware Bay. *Journal of Geophysical Research*, **96**, 7049–7064.

GEYER W. R. and R. SIGNELL (1990) Measurements of tidal flow around a headland with a shipboard acoustic Doppler current profiler. *Journal of Geophysical Research*, **95**, 3189–3197.

JOYCE T. M. (1989) On in situ "calibration" of shipboard ADCP's. *Journal of Atmospheric Oceanic Technology*, **6**, 169–172.

KING H. L., M. A. SCOTT and T. J. SMITH (1983) Some remarks on the analysis of short tidal records. *Deutsche Hydrografische Zeitschrift*, **36**, 45–59.

KOSRO P. M. (1985) *Shipboard acoustic current profiling during the Coastal Ocean Dynamics Experiment*. SIO Reference 85-8, 119 pp.

MAAS L. R. M. and J. J. M. VAN HAREN (1987) Observations on the vertical structure of tidal and inertial currents in the central North Sea. *Journal of Marine Research*, **45**, 293–318.

MÜNCHOW A., A. K. MASSE and R. W. GARVINE (1992) Astronomical and nonlinear tidal currents in a coupled estuary shelf system. *Continental Shelf Research*, **12**, 471–498.

PRANDLE D. (1982) The vertical structure of tidal currents. *Geophysical and Astrophysical Fluid Dynamics*, **22**, 22–49.

PRITCHARD D. W. (1956) The dynamical structure of a coastal plain estuary. *Journal of Marine Research*, **15**, 33–42.

REGIER L. (1982) Mesoscale current fields observed with a shipboard profiling acoustic current meter. *Journal of Physical Oceanography*, **12**, 880–886.

SANDWELL D. T. (1987) Biharmonic spline interpolation of Geos-3 and Seasat altimeter data. *Geophysical Research Letters*, **14**, 139–142.

SAUNDERS P. M. (1990) Cold outflow from the Faroe Bank Channel. *Journal of Physical Oceanography*, **20**, 29–43.

SIMPSON J. H., E. G. MITCHELSON-JACOB and A. E. HILL (1990) Flow structure in a channel from an acoustic Doppler current profiler. *Continental Shelf Research*, **10**, 589–603.